Journal of proteome research

The first whole-cell proteome- and lysine-acetylome-based comparison between Trichophyton rubrum conidial and mycelial stages

Xingye Xu, Tao Liu, Jian Yang, Lihong Chen, Bo Liu, Lingling Wang, and Qi Jin

J. Proteome Res., **Just Accepted Manuscript** • DOI: 10.1021/acs.jproteome.7b00793 • Publication Date (Web): 22 Mar 2018

ACS Publications

is published by the American Chemical Society. 1155 Sixteenth Street N.W., Washington, DC 20036

The first whole-cell proteome- and lysine-acetylome-based comparison between *Trichophyton rubrum* conidial and mycelial stages

Xingye Xu†,‡, Tao Liu†,‡, Jian Yang†, Lihong Chen†, Bo Liu†, Lingling Wang†, and Qi Jin†*

†MOH Key Laboratory of Systems Biology of Pathogens, Institute of Pathogen Biology, Chinese Academy of Medical Sciences & Peking Union Medical College, Beijing, China.

*(Q.J.) E-mail: zdsys@vip.sina.com, Telephone: +86-10-67877732, Fax: +86-10-67877736.

Email addresses:

Xingye Xu: xuxingye@ipbcams.ac.cn

Tao Liu: liutao@ipbcams.ac.cn

Jian Yang: yangj@ipbcams.ac.cn

Lihong Chen: chenlh@ipbcams.ac.cn

Bo Liu: obuil@ipbcams.ac.cn

Lingling Wang: wanglingling@ipbcams.ac.cn

Abstract

Trichophyton rubrum is the most common fungal pathogen in the world, which has been studied as an important dermatophyte model organism. Despite the prevalence of *T. rubrum*, the available antifungal therapies are not sufficiently efficient. In this study, we performed the first comparisons between the two major growth stages of *T. rubrum*: conidial and mycelial stages, based on their whole-cell proteomes and lysine acetylomes. In total, 4,343 proteins were identified in both stages, and 1,879 proteins were identified as differentially expressed between the two stages. The results showed that secretory proteases were more abundant in conidia, while aerobic metabolism and protein synthesis were significantly activated in the mycelial stage. In addition, 386 acetylated sites on 285 proteins and 5,414 acetylated sites on 2,335 proteins were identified in conidia and mycelia, respectively. The acetylation modifications were highly involved in metabolism and protein synthesis in both stages, but differentially involved in KEGG pathways and in epigenetic regulation between the two stages. Furthermore, inhibition of acetyltransferases or deacetylases significantly inhibited fungal growth and induced apoptosis. These results will enhance our understanding of the biological and physiological characteristics of *T. rubrum* and facilitate the development of improved therapies targeting these medically important pathogenic fungi.

Key words: Dermatophytes, *Trichophyton rubrum* (*T. rubrum*), proteome, label free quantification, lysine acetylation

1. Introduction

Trichophyton rubrum is a major pathogen responsible for dermatophytosis, which is the most common type of fungal infection worldwide.[1] Although *T. rubrum* often causes superficial cutaneous mycosis, deep dermatophytosis caused by this species is occasionally reported.[2] The development of effective antifungal therapies remains difficult due to inadequate tissue penetration and off-target effects.[3] Additionally, frequent relapse and anti-fungal resistance are of growing concern in dermatophyte treatment.[3] The presence of resistant structures, such as dormant fungal conidia, is another reason for failed dermatophytosis treatments.[4]

T. rubrum is a filamentous fungus with a dormant conidial stage and a vegetatively growing mycelial stage. The conidia represent a quiescent state with low metabolic activity. The primary role of the conidial stage is dispersion, in addition to providing a safe location for the fungal genome to persist in adverse environments.[5] For some pathogenic fungi, the conidia are also suggested to be involved in host recognition and infection.[5] When the conidia adhere to the host, they germinate, and a mycelium forms to establish infection. The longitudinally growing mycelia can penetrate the skin tissue and aggravate skin damage.[6] Hence, it is useful to investigate the physiological and biological properties of *T. rubrum* in each stage, which will further our understanding of this medically important fungi and facilitate the development of improved therapies targeting them.

Compared with the transcriptome, the proteome is more directly related to function and phenotype.[7] Thus, the proteome may more precisely reflect differences in

metabolism and other properties between distinct states. In addition, post-translational modifications (PTMs) can alter protein spatial structures and affect protein functions, and PTMs are reported to regulate many important cellular biological processes. Lysine acetylation is a highly dynamic and evolutionarily conserved PTM that occurs in both prokaryotic and eukaryotic organisms.[8] Histone acetylation is the leading epigenetic mechanism regulating various DNA-mediated nuclear processes.[9] Non-histone acetylation has also been found in almost every cellular compartment and regulates many vital cellular processes, including enzymatic activity, cell morphology, protein interactions and apoptosis.[10] Understanding the roles of acetylation in the biological regulation of *T. rubrum* could provide new perspectives for combating these pathogenic fungi.

T. rubrum has been studied as a model anthropic pathogenic filamentous fungus for many years. In a previous study conducted in 2008, 1,026 conidial proteins from *T. rubrum* were identified based on the analysis of expressed sequence tags (ESTs), revealing the basic proteins expressed in the dormant state of *T. rubrum*.[11] In recent years, the *T. rubrum* succinylome has been examined, leading to the identification of 569 succinylated sites on 284 proteins.[12] In the present study, we performed whole-cell proteome analysis using high-accuracy mass spectrometry to compare qualitative and quantitative differences between the conidia and mycelial stages. Our results were confirmed via parallel reaction-monitoring (PRM)-based analysis, showing highly consistent results between the two methods. Our data greatly expand our knowledge on the proteins present in the major growth stages in these fungi and

reveal significant differences between the two growth stages. The acetylome analysis showed a more widespread distribution of acetylation than succinylation in *T. rubrum*. Furthermore, acetylation was much more abundant in mycelia than in conidia. The features of and differences between the two stages were revealed through further bioinformatics analysis.

This study provides the first systematic comparison of the whole-cell proteomes of the conidial and mycelial stages and the first acetylation analysis at the whole-proteome level. Further experiments suggested that inhibition of the enzymes that control acetylation status could significantly inhibit fungal growth and induce apoptosis. This study improves our understanding the biological characteristics of the two major stages of *T. rubrum* and will contribute to the development of further strategies for combating these medically important fungi.

2. Experimental Section

2.1 Materials

All chemicals were purchased from Sigma Aldrich (St. Louis, MO, USA) unless stated otherwise.

2.2 Strains and culture

T. rubrum (strain BMU 01672) was cultured on potato dextrose agar (containing 4 g of potato starch, 20 g of dextrose and 15 g of agar in 1 L of distilled water, Becton Dickinson, Sparks, MD, USA) to obtain conidia and in sabouraud liquid medium (containing 40 g of glucose and 10 g of peptone in 1 L of distilled water) to obtain mycelia. The conidia were harvested on ice with distilled water; filtered through

cotton which was covered with gauze, and then filtered through a 400 and 600 mesh sieve sequentially. The purity of conidial sample was examined with microscope. The mycelia were harvested and washed with distilled water to remove the residual growth medium. The collected cells were frozen at -80°C for subsequent experimentation.

2.3 Protein extraction

Cells were ground in liquid nitrogen and resolved in lysis buffer containing 8 M urea, 10 mM dithiothreitol (DTT), 50 mM nicotinamide (NAM), 3 μM trichostatin A (TSA) and 0.1% protease inhibitor cocktail. Proteins were subsequently precipitated with 15% trichloroacetic acid (TCA) and then washed with cold acetone. The protein precipitate was re-dissolved in 8 M urea and 100 mM NH_4HCO_3 (pH 8.0), and the protein concentration was determined using the 2-D Quant kit (GE Healthcare, Piscataway, NJ, USA).

2.4 Trypsin digestion

Proteins were reduced with 10 mM DTT and alkylated with 20 mM iodoacetamide (IAA). The protein solution was then diluted to ensure that the urea concentration was less than 1 M, and the pH value was adjusted to 8 with NH_4HCO_3. Thereafter, the proteins were digested overnight at 37°C with trypsin (Promega, Madison, WI, USA) at a trypsin/protein ratio of 1:50 (w/w). Then, trypsin was added again, followed by incubation for an additional 4 h.

2.5 HPLC fractionation

The peptides were fractionated into 80 fractions via reverse-phase HPLC with a gradient of 2% to 60% acetonitrile (ACN) in 10 mM ammonium bicarbonate (pH 10)

over 80 min, using an Agilent 300Extend-C18 column (4.6mm × 250mm, 5-μm, 300A°, Agilent Technologies, Santa Clara, CA, USA). Then, the peptides were combined into 6 fractions for each of conidial and mycelial stage samples that would be used in the subsequent LC-MS/MS analysis of whole-cell proteome. Meanwhile, for the peptide samples that would be used for the subsequent enrichment of acetylated peptides, 3 fractions were combined for conidial stage samples and 6 fractions were combined for mycelial stage samples. In order to reduce the hydrophobicity overlap, the peptides were combined with the rules illustrated thereafter. The strategies to generate 3 total fractions after combination are illustrated as follows: final fraction 1= fraction 1+ 4+ 7+ 10…+ 79; final fraction 2= fraction 2+ 5+ 8+ 11…+ 80; final fraction 3= fraction 3+ 6+ 9+ 12…+ 78. The strategies to generate 6 total fractions after combination are illustrated as follows: final fraction 1= fraction 1+ 7+ 13+ 19…+ 79; final fraction 2= fraction 2+ 8+ 14+ 20…+ 80; final fraction 3= fraction 3+ 9+ 15+ 21…+ 75; final fraction 4= fraction 4+ 10+ 16+ 22…+ 76; final fraction 5= fraction 5+ 11+ 17+ 23…+ 77; final fraction 6= fraction 6+ 12+ 18+ 24…+ 78. All the peptide fractions were dried completely.

2.6 Affinity enrichment of lysine-acetylated peptides

Acetylated peptides were enriched via immunoprecipitation. Briefly, the fractionated peptides were suspended in NETN buffer (100 mM NaCl, 1 mM EDTA, 50 mM Tris-HCl, and 0.5% NP-40, pH 8.0) and then incubated with pre-conjugated pan antiacetyl-lysine agarose beads (PTM Biolabs, Hangzhou, China) at 4°C overnight with gentle shaking. The beads were subsequently washed with NETN

buffer four times and with ddH_2O twice. The bound peptides were eluted with 0.1% trifluoroacetic acid (TFA) and dried. The peptides were then desalted with C18 ZipTips (Millipore, Billerica, MA, USA) and finally dissolved in 0.1% formic acid (FA).

2.7 LC-MS/MS analysis

The enriched acetylated peptides and peptides digested from the whole-cell proteome were loaded in an EASY-nLC 1000 UPLC system (Thermo Fisher Scientific, Waltham, MA, USA) equipped with a Acclaim PepMap 100 reverse-phase C18 pre-column (75 μm × 2 cm, 3 μm, 100A°, Thermo Fisher Scientific, Waltham, MA, USA) and separated on a Acclaim PepMap RSLC reverse-phase C18 analytical column (75 μm × 15 cm, 3 μm, 100A°, Thermo Fisher Scientific, Waltham, MA, USA). For whole-cell proteome analysis, the gradient was 7% to 24% solvent B (0.1% FA in 98% ACN) over 40 min, followed by 24% to 38% solvent B for 14 min, then increased to 80% over 3 min and was finally held at 80% solvent B, with a flow rate of 400 nL/min. For acetylome analysis, the gradient was 7% to 25% solvent B for 26 min, followed by 25% to 40% solvent B for 8 min, and was then increased to 80% solvent B over 5 min and finally held at 80% solvent B, with a flow rate of 400 nL/min.

The eluted peptides were analyzed via Q Exactive™ Plus tandem mass spectrometry (Thermo Fisher Scientific, Waltham, MA, USA). The mass range for the MS scans was 350 to 1,800 m/z. A data-dependent procedure was adopted such that one MS scan was followed by 20 MS/MS scans. For the MS/MS scans, higher-energy

collisional dissociation (HCD) at 28% normalized collision energy (NCE) was used. The resolution for a full range mass scan was set as 70,000, and that for MS/MS scans was set as 17,500. Mass window for precursor ion selection was 2.0 m/z and charge state screening parameters were set as 2-5. Intensity threshold for triggering MS2 was 7,500 for whole-cell proteome and 5,000 for acetylome. Dynamic exclusion was set as 30s for whole-cell proteome and 15s for acetylome. Three biological replicates were performed for each sample.

2.8 Database searches

The *T. rubrum* protein database version 2 was downloaded from https://archive.broadinstitute.org/ftp/pub/annotation/fungi/dermatophytes/genomes/trichophyton_rubrum_cbs_118892/ (the database contains 11,418 sequences; commonly observed contaminants were appended to the database). The raw MS/MS data were searched using MaxQuant with the integrated Andromeda search engine (v.1.5.2.8). The mass spectra were searched against the *T. rubrum* protein database and concatenated with a reverse decoy database. This target-decoy search strategy was employed to calculate false-discovery rates (FDR).[13]

The following parameters were set for the whole-cell proteome analysis: (1) specified enzyme, trypsin; (2) maximum missed cleavages, 2; (3) maximum modifications per peptide, 5; (4) maximum charge per peptide, 5; (5) mass tolerance for precursor ions, 5 ppm; (6) mass tolerance for fragment ions, 0.02 Da; (7) static modifications, Cys carbamidomethylation; and (8) dynamic modifications, Met oxidation and acetylation at the protein N-terminus. The FDR was set as < 1% for the

peptides and proteins. The minimum peptide length was 7, and at least two peptides per protein was set as additional filter.

The following parameters were set for the acetylome analysis: (1) specified enzyme, trypsin; (2) maximum missed cleavages, 4; (3) maximum modifications per peptide, 5; (4) maximum charge per peptide, 5; (5) mass tolerance for precursor ions, 5 ppm; (6) mass tolerance for fragment ions, 0.02 Da; (7) static modifications, Cys carbamidomethylation; and (8) dynamic modifications, Met oxidation, Lys acetylation and acetylation at the protein N-terminus. The FDR of less than 1% was specified for the proteins, peptides and modification sites. The site localization probability was set to > 0.75. The minimum peptide length was 7, and the peptide scores were all above 40.

Other parameters were set as follows: max peptide mass [Da], 4,600; multiplicity, 1; and type, standard. Only protein with the best peptides match or with the best score in each protein group was reported for each MS/MS search.

2.9 Quantification of proteomic data

Label-free quantification was carried out using the MaxQuant software (version 1.5.2.8) as described previously.[13] Briefly, normalization and the intensity-based absolute quantification (iBAQ) in MaxQuant was performed on the identified peptides to quantify protein abundance. Specifically, shared peptides which matched to different protein groups were exclude from quantification. The significant differences between replicates were determined using the t-test approach. Only proteins with a fold change > 2 or < 0.5 and a p value < 0.05 in at least two biological replicates were

considered to exhibit a significant difference in protein abundance between the two stages.

2.10 PRM analysis

The peptide samples were prepared according to the whole-cell proteome analysis methodology described above. The proteins selected for PRM validation were based on the results of whole-cell proteome. In addition, to determine the target peptides of each protein selected for PRM and their retention times, the peptide sample was initially run in a DDA mode using Q Exactive™ Plus (Thermo Fisher Scientific, Waltham, MA, USA), which was coupled to the UPLC online with the identical gradient to subsequent PRM analysis. Based on the results of this pre-experiment, a total of 54 peptides were selected and input as entries into the inclusion list, which would be detected in the PRM assay. The details of the inclusion list are shown in Table S1.

In the subsequent PRM analysis, the peptide mixture was loaded onto an PicoFrit capillary column (75μm× 15 cm, New Objective, Woburn, MA, USA) packed with ReproSil-Pur Basic C18 reverse-phase resin (1.9 μm, 100A°, Dr. Maisch GmbH, Ammerbuch, Germany) and separated in an EASY-nLC 1000 UPLC system (Thermo Fisher Scientific, Waltham, MA, USA), with a gradient of 6% to 23% solvent B (0.1% formic acid in 98% ACN) over 38 min, followed by 23% to 35% solvent B over 14 min and increasing to 80% solvent B over 4 min, with a flow rate of 400 nL/min. The eluate was examined via mass spectrometry using Q Exactive™ Plus (Thermo Fisher Scientific, Waltham, MA, USA), which was coupled to the UPLC online. After a

full-scan event, the MS/MS scans in PRM mode were triggered by inclusion list. A full mass spectrum was detected in the Orbitrap at a resolution of 70,000 (AGC target was set as $3E^6$; the maximum injection time was 50 ms; and the m/z range was 350–1200), followed by 20 MS/MS scans on the Orbitrap at a resolution of 17,500 (AGC target was $1E^5$, and the maximum injection time was 100 ms) in a data-independent procedure. Mass window for precursor ion selection was 1.6 m/z. The isolation window for MS/MS was set at 2.0 m/z. The NCE was 27% with HCD. Three biological replicates were performed.

PRM data were analyzed using Skyline (v.3.6) software. The following parameters were set for this analysis: (1) enzyme, trypsin [KR/P]; (2) max missed cleavages, 0; (3) peptide length, 7-25; (4) static modification, Cys carbamidomethyl; (5) variable modification, Met oxidation; and (6) max variable modifications, 3. The following transition settings were used: (1) precursor charges, 2 and 3; (2) ion charges, 1 and 2; (3) ion types, b, y and p; (4) product ions, from ion 3 to the last ion; and (5) ion match tolerance, 0.02 Da.

2.11 Quantitive real time PCR (qRT-PCR) assay

The conidia and mycelia of *T. rubrum* were grinded in liquid nitrogen, and total RNA were isolated using RNeasy Plant Mini Kit (Qiagen, Hilden, Germany) according to manufacturer's protocol. mRNA were reverse-transcribed to cDNA using SuperScript III First-Strand kit (Invitrogen, Carlsbad, CA, USA). The primer sequences were listed in Table S2. The qRT-PCR was performed in an ABI StepOne Plus (Applied Biosystems, Foster City, CA, USA). mRNA relative expression was

normalized to β-tubulin and calculated using the $2^{-\Delta\Delta CT}$ method.

2.12 Western blotting

Proteins were separated in a 12% SDS-PAGE gel and transferred to a PVDF membrane (Bio-Rad Laboratories, Hercules, CA, USA), which was then incubated in blocking buffer for 2 h. The membrane was subsequently incubated with pan anti-acetyllysine antibodies, anti-histone H4 antibodies and two histone lysine acetylation site-specific antibodies (anti-H4K17acetyl antibody and anti-H4K78acetyl antibody) (PTM Biolabs, Hangzhou, China) overnight at 4°C. Incubation with the horseradish peroxidase-conjugated goat-anti-rabbit secondary antibody was then performed for an additional 2 h at room temperature.

2.13 Bioinformatics analysis

Gene Ontology (GO) annotations were derived from the UniProt-GOA database (www. http://www.ebi.ac.uk/GOA/) and complemented with InterProScan soft. The proteins were classified separately according to biological processes, cellular components and molecular functions. Subcellular localization was predicted using WoLF PSORT software. Pathways were annotated using the Kyoto Encyclopedia of Genes and Genomes (KEGG) database.

Enrichment analysis of the identified proteins was performed using the two-tailed Fisher's exact test for each category to analyze the functional enrichment or depletion of the identified proteins compared with all of the proteins in the database. The terms with p values of less than 0.05 were considered significant.

Amino acid sequence models surrounding the acetylated lysines were analyzed using motif-X. The secondary structural properties of the acetylated lysine residues were determined using NetSurfP.

2.14 Fungal proliferation and viability assay

Three acetytransferase inhibitor: C646, MG149, Remodelin, and three deactylase inhibitor: Panobinostat (LBH 589), Trichostatin A (TSA), Salermide were all purchased from Selleck Chemicals (Houston, TX, USA). The *T. rubrum* (1 to 3 × 10^5 CFU/mL) were inoculated in the RPMI 1640 medium (Gibco, Grand Island, NY, USA) and incubated with different concentrations of each inhibitor (ranging from 0 to 100 μM in 0.1% DMSO) at 28°C for 7 day. The fungal viability was examined using XTT cell proliferations assay kit (Abnova, Taipei, Taiwan) according to the manufacturer's protocol. Briefly, 10 μl of XTT was added to 100 μl culture and incubated for 3 h. The absorbance of each sample was measured using an infinite M200 pro microplate reader (TECAN, Mannedorf, Switzerland) at a wavelength of 450 nm.

2.15 Determination of minimum inhibitory concentration (MIC) and minimum fungicidal concentration (MFC)

MIC and MFC were used to evaluate the fungistatic and fungicidal effects of each inhibitor according to the M38-A microdilution technique proposed by the Clinical and Laboratory Standards Institute (CLSI).[14] MIC was defined as the lowest concentration of inhibitor that completely inhibited the fungal growth. MIC was determined with XTT assay described above and coupled with microscopic

examination.

The liquid in each well which shown the inhibition in MIC test were inoculated on the sabouraud dextrose agar (containing 5 g of peptic digest of animal tissue, 5 g of pancreatic digest of casein, 40 g of dextrose and 15 g of agar, Becton Dickinson, Sparks, MD, USA) and incubated at 28°C. The MFC was determined as the lowest concentration of no growth on the plate. Each assay was carried out with three replicates.

2.16 TUNEL assay and nuclear staining

Fungi conidia were cultured in liquid medium for 12-14 h to form mycelia and then treated with each inhibitor at MIC in RPMI 1640 medium for 2 h. Apoptosis was analyzed by DeadEnd Fluorometric TUNEL System (Promega, Madison, WI, USA) as described previously.[15] Briefly, The mycelia were fixed by treatment with 3.7% formaldehyde for 1 h, and the cell wall was digested with lyticase for 30 min. Cell were permeabilized with 0.1% Triton X-100 and 0.1% sodium citrate for 2 min on ice, and then stained with both TUNEL and DAPI according to the manufacturer's guidelines. The cell were visualized with Eclipse TE-2000U fluorescence microscopy (Nikon, Tokyo, Japan). Three replicated experiments were performed.

2.17 Annexin V-FITC/PI staining

Due to the existence of cell wall, fungal could not been stained with Annexin V-FITC; therefore, protoplasts were generated. Mycelia were washed with PBS and digested using *Trichoderma harzianum* lysing enzymes in 1.5 M sorbitol buffer (pH 7.0) to obtain protoplasts as described previously.[16] Protoplasts were treated with each

inhibitor at 0.5 MIC for 2 h and double stained with propidium iodide (PI) and Annexin V-FITC using the Annexin V-FITC Early Apoptosis Detection Kit (Cell Signaling Technology, Danvers, MA, USA). Samples were analyzed on a BD FACSCanto II flow cytometer (BD Biosciences, San Jose, CA, USA).

3. Results

3.1 Whole-cell proteomic comparison between the conidial and mycelial stages in *T. rubrum*

Based on a shotgun proteomics approach, a total of 4,343 proteins were identified in both stages, based on 39,662 unique peptides. Three biological replicates were performed for the conidial and mycelial stages. An FDR < 0.01 and at least two unique peptides per protein were considered to indicate confident identification of proteins.

3.1.1 GO classification of the conidial and mycelia proteomes

In total, 3,926 and 4,099 proteins were identified in the conidial and mycelial stages, respectively. The GO classifications for the conidial- and mycelial-stage proteomes are shown in Figure S1. The proteins presented a similar distribution in conidia and mycelia based on the GO classification. In the biological process classification, most proteins were observed to be involved in metabolic processes, cellular processes and single-organism processes. In the molecular function classification, the majority of the proteins were involved in the binding and catalytic activity categories. In the cellular component classification, most of the proteins are classified into the cell, organelle, macromolecular complex and membrane categories.

3.1.2 Qualitative and quantitative comparison of proteins between the conidial and mycelial stages

In total, 244 and 418 proteins were specific to the conidial and mycelial stages, respectively. Additionally, 3,681 proteins were common to the two stages. Based on the criteria of $p < 0.05$ and a fold change > 2 or < 0.5 for proteins in at least two biological replicates to be considered significantly differentially expressed, a total of 1,879 proteins were identified as differentially expressed proteins (DEPs). Among these proteins, 1,612 were up-regulated, and 267 were down-regulated in the mycelial vs. the conidial stage (Table S3). The ratio of protein abundance for all the quantified proteins in the mycelial vs. the conidial stage is shown in Figure S2. The reproducibility of quantification is shown in Figure S3, demonstrating that the three replicates were highly reproducible.

3.1.3 GO enrichment of stage-specific proteins and differentially expressed proteins

The results of enrichment analysis were shown in Figure 1 and Table S4. Regarding the enrichment of conidium-specific proteins based on biological processes, carbohydrate metabolic processes and nitrogen cycle metabolic processes were significantly enriched. Regarding the enrichment of proteins that were down-regulated in the mycelial vs. the conidial stage based on biological processes, the categories such as oxidation-reduction process, single-organism carbohydrate metabolic process, proteolysis and pentose-phosphate shunt were enriched. The proteins in the pentose-phosphate shunt category were enzymes involved in the pentose phosphate

pathway. Specifically, 6-phosphogluconate dehydrogenase, the rate-controlling enzyme in the pentose phosphate pathway, was down-regulated in the mycelial vs. the conidial stage, indicating that the pentose phosphate pathway is more abundant in the conidial vs. the mycelial stage. Similar results have been obtained in the pathogenic fungus *P. brasiliensis*.[17]

In the molecular function classification, the protease activity category was significantly enriched in both conidium-specific proteins and proteins that were more abundant in the conidia, in categories including serine-type peptidase activity, peptidase activity and endopeptidase activity. Most of the proteins in these categories are secreted proteases. Secreted proteinases, and particularly serine proteases, are considered to be critical virulence factors for dermatophytes, which degrade keratinized structures in the skin, nails and hair as their sole source of carbon and nitrogen during infection.[18] Our data showed that pathogenicity-related secreted proteases were more abundant in conidia. In accordance with this result, the adhesin protein (TERG_02242T0), which facilitates binding to the host stratum corneum in the early stages of infection, was also identified as being overexpressed in conidia vs. mycelia. These results may suggest a possible role for these proteins in the adherence and infection of *T. rubrum* conidia.

In the enrichment analysis of mycelium-specific proteins based on biological processes, cofactor biosynthetic processes and lipid metabolic processes were significantly enriched. According to molecular function, the mycelium-specific proteins were significantly enriched for nuclease activity, 3'-5' exonuclease activity

and exonuclease activity. Additionally, N-acetyltransferase activity and acetyltransferase activity were enriched in the mycelium-specific stage, indicating that protein acetylation modifications are more extensive in the mycelial stage. Membrane components were enriched in the cellular component category for mycelium-specific proteins.

In the GO enrichment analysis of proteins that were up-regulated in the mycelial vs. the conidial stage, most proteins were enriched for the ribosome, eukaryotic translation initiation factor 3 complex, and large ribosomal subunit categories of cellular components. Additionally, in the molecular function category, most proteins were enriched for the structural constituent of ribosome, structural molecule activity, translation factor activity, RNA binding and translation initiation factor activity categories. In accordance with these results, translation and peptide biosynthetic processes were enriched among the biological processes. The processes indicated above suggest that protein synthesis is significantly enhanced in the mycelial stage. Additionally, in the biological process classification, cellular respiration, aerobic respiration, the tricarboxylic acid cycle, tricarboxylic acid metabolic processes and citrate metabolic processes were enriched, suggesting that respiratory metabolism is up-regulated in mycelia. Besides, ion transmembrane transporter activity was significantly enriched based on molecular function classification, including inorganic cation transmembrane transporter activity, hydrogen ion transmembrane transporter activity, monovalent inorganic cation transmembrane transporter activity and cation transmembrane transporter activity.

3.1.4 KEGG enrichment of stage-specific proteins and differentially expressed proteins

In the KEGG enrichment analysis of conidium-specific proteins and proteins that were more abundant in the conidia (Figure S4 and Table S5), in addition to the pentose phosphate pathway mentioned above, starch and sucrose metabolism and nitrogen metabolism were significantly enriched. Two categories of microbial metabolism in diverse environments and biosynthesis of secondary metabolites were also significantly enriched in conidia. Secondary metabolites are a group of small organic molecules that are not essential for growth, but facilitate organism to survive under certain conditions.[19] Some secondary metabolites also shown to contribute to fungal pathogenicity.[20] The proteins in these two categories may facilitate the survival of conidia under adverse conditions. In the KEGG enrichment analysis of proteins showing greater abundance in mycelia, the ribosome, TCA cycle and oxidative phosphorylation categories were significantly enriched, which supported the results of the GO enrichment analysis, suggesting that protein synthesis and aerobic metabolism are more active in mycelia.

3.1.5 Other DEPs in the conidial and mycelial stages

In addition to the proteins identified in the enrichment analyses described above, two other categories of proteins drew our attention. One of these categories was cytoskeleton and molecular motor proteins, which were overexpressed in mycelia vs. conidia. The cytoskeleton and molecular motor systems are essential for shuttling vesicles and organelles, cellular division, and hyphae elongation.[21] Microtubules and

actin filaments are the two major constituents of the cytoskeleton. Microtubules polymerize from tubulin dimers. All four tubulin proteins identified in our study (TERG_02189T0, TERG_03906T0, TERG_07773T0 and TERG_07904T2) were up-regulated in the mycelial vs. the conidial stage. Actin filaments polymerize from actin monomers. Six actin-related proteins (TERG_00111T0, TERG_00195T0, TERG_00534T0, TERG_00808T0, TERG_01650T0 and TERG_04413T0) were up-regulated, and one protein (TERG_06946T0) showed no significant difference between conidia and mycelia. Septins are GTP-binding proteins that polymerize to form filaments. Septin filaments co-localize with microtubules and actin filaments, suggested to regulate their stability and activity.[22] Four septins (TERG_03608T0, TERG_04514T0, TERG_046776T0 and TERG_07865T1) were overexpressed in mycelia vs. conidia, while one septin (TERG_02382T0) did not show any significantly difference in expression between the two stages. Moreover, kinesin, dynein and myosin, which are the major molecular motor proteins, were also significantly more abundant in the mycelial vs. the conidial stage.

The other category of proteins that drew our attention was heat shock proteins (HSPs), which were also significantly overexpressed in the mycelial vs. the conidial stage. In our study, a total of fourteen HSPs were found to be up-regulated in the mycelial vs. the conidial stage, including seven Hsp70 family proteins (TERG_01002T0, TERG_01883T0, TERG_03037T0, TERG_03206T0, TERG_07041T0, TERG_07058T0 and TERG_07658T5), three HSP40 proteins (TERG_03062T0, TERG_05280T0 and TERG_06104T0), Hsp12 (TERG_01122T0),

Hsp90 (TERG_06963T0), HSP60 (TERG_04141T0), and HSP78 (TERG_07949T0). Additionally, one HSP30/Hsp42 (TERG_01659T0) protein was specific to the mycelial stage. Only one HSP protein, HSP31 (TERG_00228T0), was found to be specific to the conidial stage, and no HSPs were more abundant in conidia compared with mycelia. Each HSP responds to specific conditions and cooperates with other HSPs to support the survival of fungi under environmental challenges.[23] Thus, the precise biological roles of each of these HSPs require further investigation.

3.1.6 PRM-based validation and qRT-PCR assay

A PRM assay was performed to confirm the whole-cell proteome results. A total of 14 proteins were confirmed, including 8 up-regulated proteins and 4 down-regulated proteins identified based on label-free quantitative analysis and 2 proteins that were only identified in the conidial stage. These proteins were selected for their functional significance concluded from proteome analysis, and the ratio of protein abundance varied in a wide range. The fold-change values for these proteins indicated by the PRM results are presented in Table 1 and Table S1. The PRM and label-free quantification results were highly consistent, especially for the two proteins specific to the conidial stage (TERG_00216T0 and TERG_06780T0), indicating confidence in the whole-cell proteome results.

A total of 24 secondary metabolism- related proteins were down-regulated in mycelial vs. conidial stage based on label free quantification. We randomly selected 14 of these secondary metabolism- related proteins for qRT-PCR assay to investigate the relative mRNA expression level for these proteins. The results shown that mRNA

expression level of most of these selected protein were down-regulated in mycelia vs. conidia stage (Figure S5).

3.2. Proteome-wide analysis of lysine acetylation in the conidial and mycelial stages of *T. rubrum*

The lysine acetylome of *T. rubrum* has not been reported previously. In this study, we performed acetylome analysis on the two major growth stages (conidia and mycelia) in the *T. rubrum* life cycle.

3.2.1 Identification of whole-cell lysine acetylation in *T. rubrum*

In total, 5,580 acetylated sites on 2,422 proteins were identified in the two stages. A total of 386 acetylated sites were identified on 285 proteins in conidia, and 5,414 acetylated sites were identified on 2,335 proteins in mycelia (Figure S6, Figure S7A and Table S6).

The identified acetylated proteins accounted for 23.25% of the *T. rubrum* proteome. This percentage is higher than in the acetylomes of several other fungi reported recently, such as *C. albicans* (5.28%),[24] *S. cerevisiae* (15.77%),[25] *P. soja*e (6.04%)[26] and *B. cinerea* (5.75%)[10]. The average number of acetylated sites per protein in *T. rubrum* was 2.3, and 49% of the identified acetylated proteins possessed only one acetylated site, while 22% possessed two, and 29% possessed three or more acetylated sites (Figure S7B).

3.2.2 GO and subcellular localization classification of the acetylated proteins

To further investigate the lysine acetylome in each *T. rubrum* stage, we performed GO classification of the identified acetylated proteins (Figure 2 and Table S7). Based

on the biological process categorization, the distribution of acetylated proteins was almost the same in the conidial and mycelial stages. The three largest classes were metabolic processes (34.8% in conidia, 33.5% in mycelia), cellular processes (26.1% in conidia, 29.0% in mycelia) and single-organism processes (23.0% in conidia, 20.6% in mycelia). Based on the molecular function classification, the percentage of catalytic activity decreased from 47.3% to 39.6% in the conidial vs. the mycelial stage, while the percentage of binding increased from 39.3% to 49.3%. In the cellular component category, the two stages exhibited a similar acetylation distribution, and cell, organelle, macromolecular complex and membrane were the four major categories.

In the subcellular localization analysis, the three largest categories were cytosol, nuclear and mitochondria in both the conidial and mycelial stages. The percentage of acetylated proteins located in the cytosol was 36.1% in conidia and 21.6% in mycelia; the percentage located in the nucleus was 21.4% in conidia and 37.1% in mycelia; and the percentage located in the mitochondria was 19.3% in conidia and 23.5% in mycelia. Compared with the succinylome analysis that we conducted in a previous study, mitochondria was the major category for succinylated proteins, which demonstrates the different features of these two PTMs depending on subcellular localization.

3.2.3 GO and KEGG enrichment analysis of acetylated proteins.

GO enrichment analysis was performed to better understand the functions of the identified acetylated proteins (Figure S8 and Table S8). The acetylated proteins

showed similar enrichment in the conidia and mycelia based on the GO analysis. According to biological process enrichment, various metabolic processes, translation and macromolecule biosynthetic processes were greatly enriched for acetylated proteins. Metabolic processes such as oxoacid metabolic processes, carboxylic acid metabolic processes, organic acid metabolic processes, and cellular amino acid metabolic processes were enriched in both the conidial and mycelial stages. Additionally, translation and gene expression were significantly enriched in both stages. In agreement with this observation, the molecular function enrichment analysis showed a significant enrichment for structural constituents of ribosome and translation factor activity. Accordingly, in the analysis of cellular component enrichment, the greatly enriched categories included the ribosome and ribonucleoprotein complex categories. In other organisms, such as *S. japonicum*,[27] *E. coli*,[8] and *M. abscessus*,[28] acetylation occurs on ribosomal proteins, suggesting that it plays a conserved role in the ribosomes and during translation.

In the KEGG enrichment analysis of acetylated proteins, the ribosome, propanoate metabolism, carbon fixation pathways in prokaryotes and systemic lupus erythematosus pathways were enriched in both the conidial and mycelial stages. In addition, metabolic pathways such as pyruvate metabolism, methane metabolism and the pentose phosphate pathway were specifically enriched in the conidial stage. Furthermore, three categories related to secondary metabolism were enriched for acetylated proteins in the conidial stage, including biosynthesis of secondary metabolites, microbial metabolism in diverse environments and biosynthesis of

antibiotics. In the mycelial stage, the spliceosome, alpha-linolenic acid metabolism and biosynthesis of unsaturated fatty acids were specifically enriched.

3.2.4 Acetylation of proteins related to fungal pathogenicity

A total of 272 proteins that have been reported to be related to pathogenicity in *T. rubrum* or other fungi to our knowledge were found to be acetylated in the present study (Table S9). Of these pathogenicity-related proteins, 22 proteins were only acetylated in conidia; 224 were only acetylated in the mycelial stage; and 26 were acetylated in both stages. *T. rubrum* is a highly specialized pathogenic fungus that exclusively infects skin, hair and nails; thus, secreted proteases that can degrade host keratin are important for its virulence.[29] Our analysis identified 25 endo- and exo-proteases that were acetylated, such as alkaline serine proteases, aspartic endopeptidase Pep2 and carboxypeptidase Y homolog A. In addition to secreted proteases, proteins involved in responses to environmental stress are also related to fungal pathogenicity.[30] According to our results, 11 heat shock proteins (including HSP70, HSP90, HSP31 and HSP12), 1 superoxide dismutase, 2 peroxidases, 2 pH signal transduction proteins (PalH22 and PalA) and 7 other stress response proteins were found to be acetylated. Many of these pathogenic determinants lack an N-terminal signal peptide and are transported through unconventional secretion pathways, which appear to be involved in host-pathogen interactions.[31] One group of acetylated proteins was involved in this secretion pathway, including exocyst complex component, endosomal cargo receptor, vacuolar protein sorting-associated, SNARE Ykt6 and SNF7 family proteins. Additionally, the membrane transporters

belonging to two superfamilies, the ATP-binding cassette superfamily (ABC) and the major facilitator superfamily (MFS), which are related to pathogenesis and multidrug resistance, have been studied in *T. rubrum* and other fungi.[32] In the present study, a total of 21 acetylated proteins belonging to these two membrane transporters superfamilies were identified. In addition to the proteins mentioned above, 82 proteins involved in pathogenicity-related signaling transduction pathways, 25 proteins involved in the synthesis and maintenance of the membrane and cell wall and 55 proteins involved in secondary metabolism, autophagy, components of the proteasome, ubiquitin-mediated protein turnover and degradation were also found to be acetylated. Further studies are needed to investigate whether acetylation plays a role in *T. rubrum* pathogenicity; such studies will be informative for improving therapies targeting these medically important fungi.

3.2.5 Histone acetylation

The dynamic modification of histone acetylation plays essential roles in regulating gene transcription by altering chromatin accessibility.[33] Histone acetylation is also essential for processes such as DNA replication, DNA repair, accurate genome organization and gene regulation, which are all essential for organism growth and pathogenicity.[34] In *T. rubrum*, 42 acetylated sites were identified on histones, including H2A, H2B, H3, H4, and two histone variants (H2A.Z and H3.variant). H2B exhibited 15 acetylated sites, making it the most heavily modified histone in *T. rubrum*. Most of the acetylated sites identified on histones are conserved in other organisms (Figure 3A).[35-37] In the comparison of histone acetylation between the two

stages, more acetylated sites on histones were observed in mycelia than in conidia. A total of 20 acetylated sites were common to the two stages, and 22 acetylated sites were specific to the mycelial stage. The different acetylation profiles of the histones between the two stages indicated that acetylation is differentially involved in epigenetic regulation in these two stages. Two acetylated sites were validated via western blot analysis, which were consistent with the MS results showing that H4K78 was specific to mycelia, and H4K17 was common to the two stages (Figure 3B). As found in our previous study of lysine succinylation in *T. rubrum*, a total of seven succinylated sites were identified on histones, which was much smaller than the number of acetylated sites. Four sites on histones (H3K57, H3K80, H4K60 and H4K92) were both acetylation and succinylation targets. The differences in the acetylation and succinylation modifications on histones suggest that these two PTMs participate differently in epigenetic regulation. It will be interesting to investigate the specific roles of these two PTMs.

3.2.6 Motif analysis of acetylated sites

We examined the sequences surrounding the identified acetylated lysine sites (Kac) to define acetylation site motifs (10 amino acids upstream and 10 amino acids downstream of the Kac) using the Motif-X program. In the conidial stage, 6 significantly enriched and conserved motifs were identified based on 272 unique acetylated sites. In the mycelial stage, 17 conserved motifs were identified based on 4,887 acetylated sites (Table S10). Some of these motifs, such as $K_{ac}Y$, $K_{ac}F$, $K_{ac}H$, and K_{ac}***K, are conserved in other species.[10, 26, 27]

A heat map (Figure 4) was generated to show the enrichment or depletion of specific amino acids neighboring the Kac sites. In both stages, the amino acids aspartate (D), glutamate (E), phenylalanine (F), glycine (G), histidine (H) and isoleucine (I) were found to be relatively biased toward being present around Kac sites. In the mycelial stage, lysine (K) and arginine (R) were greatly enriched surrounding Kac sites, but were greatly depleted in the -5 to -1 positions. Alanine (A), cysteine (C) and valine (V) were also more abundant around Kacs in mycelia than in conidia. However, tyrosine (Y) at the +1 position was more abundant in conidia than in the mycelial stage. These different preferences for amino acids around Kac sites reflects the specific recognition of enzymes that catalyze acetylation in each stage. Further studies are needed to investigate whether the different types of enzymes that regulate acetylation are active in these different growth stages.

3.2.7 Secondary structure characteristics of the acetylated sites

In the secondary structure analysis shown in Figure 5, acetylated lysines are similarly distributed in α-helices (45.1%) and coils (44.6%). In *C. albicans*[24] and *S. japonicum*,[27] acetylated sites are more biased toward being located in coils than in α-helices, but in *M. tuberculosis*,[38] acetylated sites are biased toward being located in α-helices over coils. These differences in acetylated lysines in the distribution of secondary structures may be due to the specificities of each species. Acetylated sites are least abundant in β-strands that are conserved in the above species. Furthermore, acetylated lysines were found to be less likely to be exposed on the protein surface than all lysines, which is consistent with results from *B. cinerea*.[10] This bias differs

from the pattern observed for *T. rubrum* succinylation, in which succinylated lysines tended to be exposed on the protein surface compared with all lysines, suggesting distinct properties for each PTM.

3.2.8 Conservation of acetylated proteins in other species

To determine whether the acetylated proteins identified in *T. rubrum* were conserved in other organisms, we compared the *T. rubrum* acetylome to previously reported acetylation analyses from other species (Table S11). The overlap in acetylated proteins between *T. rubrum* and other species is shown in Figure 6. In total, 118 homologous acetylated proteins were observed in the *E. coli* acetylome,[8] 659 in the yeast acetylome,[25] 536 in the mouse acetylome,[39] 510 in the human acetylome[39] and 249 in the *C. albicans* acetylome.[24] The percentages of homologous acetylated proteins in yeast (61.6%) and *C. albicans* (52.2%) were much higher than in *E. coli* (35%), mouse (41.7%) and human (41.2%), which may occur because the two fungi species are more closely genetically related to *T. rubrum* than the other species.

3.2.9 Cross-talk between acetylation and succinylation in *T. rubrum*

In our previous study, 569 succinylated lysine sites were identified on 284 proteins.[12] These succinylated proteins were shown to be involved in various key cellular processes. When the acetylated proteins identified in our study were compared with the succinylated proteins, 231 proteins and 257 sites were found to overlap between these two PTMs (Table S12). This finding suggested that 81.34% of the succinylated proteins and 45.17% of the succinylated sites were simultaneously modified by acetylation. To further investigate the relationship between acetylation

and succinylation, the modified proteins were classified into four types and subjected to KEGG pathway enrichment analysis (Figure 7). Type 1 included locations where succinylation and acetylation modify the same site. Many important metabolic pathways were enriched in this category, including pyruvate metabolism, glycolysis/gluconeogenesis and the citrate cycle (TCA cycle). Type 2 included locations where acetylation and succinylation modifications are present on the same protein, but not at the same position. This category of proteins mainly participated in the biosynthesis of unsaturated fatty acids, fatty acid degradation and the lysosome. Type 3 consisted of proteins that are only acetyl-modified, while type 4 consisted of proteins that are only succinyl-modified. Galactose metabolism, the spliceosome and DNA replication were specifically enriched in type 3, while cardiac muscle contraction and the non−alcoholic fatty liver disease (NAFLD) pathway were enriched in type 4. The proteins belonging to types 1 and 2 suggest that acetylation and succinylation are co-regulated in several basic biological processes, although these two modifications also play some specific roles, as shown by types 3 and 4.

3.2.10 Global comparison of acetylation levels and protein abundance

Acetylation was much more abundant in mycelia than in conidia. In addition to the greater number of acetylated proteins found in mycelia (2,335 in mycelia compared with 285 in conidia), the number of acetylated sites per protein was 2.32 in mycelia, compared with 1.35 in conidia. In the whole-cell proteome analysis, most differentially expressed proteins were observed to be more abundant in mycelia vs. conidia. Thus, we sought to examine whether the differences in acetylation levels

between the two stages are correlated with protein abundance. Hence, the acetylomes were compared with the proteomes of the two stages. Among the conidium-specific acetylated proteins, 12 proteins were identified only in the conidial stage in the whole-cell proteome analysis, which may be due to specific protein expression in the conidial stage. Moreover, 14 conidium-specific acetylated proteins were shown to be more abundant in the conidial stage, while 12 showed no significant differences in protein abundance between the two stages, and 5 were more abundant in the mycelial stage. Regarding the mycelium-specific acetylated proteins, 108 were identified only in the mycelial stage; 894 were more abundant in the mycelial stage; 632 showed no significant differences in protein abundance; and 54 were more abundant in the conidial stage.

Furthermore, 198 acetylated proteins were common to the conidial and mycelial stages, 157 of which were modified with more acetylated sites in mycelia than in conidia. Compared with the whole-cell proteome, 83 of the 157 proteins were more abundant in mycelia, while 39 showed no significant differences in protein abundance, and 10 proteins were more abundant in the conidial stage. Meanwhile, 4 proteins exhibited more acetylation sites in conidia than in mycelia. Of these proteins, 1 was more abundant in conidia, and 1 was more abundant in mycelia.

These results showed a slight bias, in that acetylation modifications tended to be identified on relatively more-abundant proteins between the two stages, although there were no significant correlations regarding acetylation and protein abundance.

This observation led to the conclusion that the differences in acetylation levels between the two stages were not the result of protein abundance.

3.2.11 Effect of acetyltransfrases and deacetylases inhibition on fungal viability and induction of apoptosis

Since the acetylated proteins were shown to be involved in essential biological processes in *T. rubrum*, we sought to investigate the importance of normal acetylation status on the growth and viability of these fungi. Acetylation status is controlled by two types of enzymes: lysine acetyltransferases (KATs) and lysine deacetylases (KDACs). Inhibition of KATs or KDACs would lead to disordered acetylation status. Inhibitors of KATs or KDACs had been shown to inhibit growth of cancer cell and induced cell apoptosis.[40, 41] Some of these inhibitors had also been suggested to effectively inhibit fungal growth.[42] In this study, we tested six inhibitors of KATs and KDACs for their impact on *T. rubrum*.

Of the six tested inhibitors, C646 and salermide did not shown obvious effect on inhibition of fungal growth, thus had not been used in the subsequent analysis. The other four inhibiotrs: MG149, remodelin, LBH589 and TSA were found to be effective to reduce viability of *T. rubrum*. These inhibitors showed significant fungistatic effect in a dose-dependent manner (Fig. 8A). In addition, MIC and MFC were determined for each inhibitor as shown in Table 2. TSA shown the lowest MIC (5 μM) that completely inhibit fungal growth, while TSA and MG149 shown the minimum fungicidal effects at 20 μM and 30 μM respectively.

To investigate whether cell apoptosis could be induced in *T. rubrum* by treatment of

KATs or KDACs inhibitors as suggested in mammalian cell, TUNEL assay was performed to detect DNA fragmentation during apoptosis. As shown in Fig. 8B and 8C, mycelia treated with 0.1% DMSO (control) did not show obvious fluorescent signal after TUNEL staining. In contrast, significant TUNEL positive green fluorescence was observed in inhibitors treated samples, suggested apoptosis was occurred with the treatment of inhibitors.

In apoptotic cells, phosphatidylserine (PS) was translocated from the inner to outer leaflet of the plasma membrane, thereby exposing PS to the external cellular environment. Annexin V has a high affinity for PS, therefore fluorochromes-conjugated Annexin V was served as a sensitive probe of cell that are undergo apoptosis.[43] In addition, Annexin V coupled PI stain could distinguish between apoptotic and necrotic cell. As shown in Fig. 8D, all the four inhibitors treatment could induce cell apoptosis. TSA shown the most significant effect on inducing cell apoptosis, that 14.8% of the cell were underwent early apoptosis (Q4, Annexin V-FITC+/PI-), 4.5% of the cell were underwent late apoptosis (Q2, Annexin V-FITC+/PI+). Both TSA and LBH589 treatment also induced a certain proportion of necrotic cell (Q1, Annexin V-FITC-/PI+), of which the percentage was 5.4% and 5.2% respectively.

4. Discussion

In this study, we performed the first comparative, high-throughput analysis of the proteomes and acetylomes of the two major growth stages in the *T. rubrum* life cycle. Obtaining pure sample of each stage was the basis for subsequent comparison

between the two stages. For filamentous fungi, prevent contamination of mycelial fragments is the essential step in conidia sample preparation. In our study, we filtered the collected conidia through the cotton which was covered with gauze, before the subsequent filter step using 400 and 600 mesh sieve. With this approach, the conidial samples could be considered 100% pure based on microscopic examination.

In 2008, the conidia proteome was examined, which led to the identification of 1,026 proteins based on the EST database.[11] With the development of accurate mass spectrometry methods and the availability of the *T. rubrum* genome annotation, many more proteins were identified in our study, leading to a total of 3,926 conidial proteins. Although conidia are considered to represent a dormant state, with low metabolism and inhibited protein expression, our study showed that most proteins (84.8%) were common to the conidial and mycelial stages. Thus, the conidial proteome is more complex than previously thought, suggesting that the proteins exhibit functions in *T. rubrum* conidia other than simply maintaining their quiescent status. This finding is consistent with the hypothesis that the enzymes required for nearly all biological processes are already present in conidia, which allows rapid initiation of vegetative growth when a source of nutrition is encountered.[5]

Our results also showed that some secretory proteases and adhesion proteins related to infection were more abundant in the conidial stage. These results indicate that although the conidia are in a dormant state, relatively high levels of virulence proteins are expressed in conidia. It is possible that when the fungus comes into contact with a host, these proteases may immediately be extracellularly secreted to promote skin

tissue adherence and degradation to establish an infection, although further experiments are needed to confirm this hypothesis. Moreover, microbial metabolism in diverse environments and secondary metabolism-related proteins were significantly enriched among the conidium-specific proteins and proteins that were more abundant in the conidia, suggesting that these proteins may contribute to the ability of conidia to survive under adverse conditions.

In the present study, proteins related to aerobic respiration, cellular respiration and the citrate cycle (TCA cycle) were all significantly up-regulated in the mycelial stage. Consistently, mitochondrial proteins were significantly increased in the mycelial stage according to the subcellular localization classification (Table S3), suggesting that aerobic respiration is more active in mycelia. Additionally, the pentose phosphate pathway was down-regulated in mycelia vs. conidia. These results suggest a transition from fermentation metabolism to respiration metabolism during the transition from the conidial to the mycelial stage. Similar results have been obtained in other fungi.[17] Fermentative metabolism is the major pathway providing energy in conidia, with a shift occurring to respiratory metabolism in the mycelial stage when the respiratory machinery is completely constructed. Our results also showed that protein expression levels were greatly increased in the transition from the conidial to the mycelial stage. All of these results suggest that the mycelium is a vigorous growth stage, with increased protein synthesis and efficient metabolism.

Cytoskeletal proteins, along with their respective molecular motors and other associated proteins, play important roles in hyphal growth.[21] It is reasonable that most cytoskeletal

and motor proteins were found to be specific to or more abundant in the mycelial stage, indicating the increased need for these proteins in the vegetatively growing mycelial stage. In addition, HSPs showed a significant up-regulation in the mycelial vs. the conidial stage. HSPs are a group of proteins that respond to shifts in temperature and various environmental stresses. In fungi, HSPs are also implicated in phase transition, antifungal drug resistance, pathogenicity and fungal virulence.[44] For example, HSP90 has been suggested to be involved in pathogenicity and drug susceptibility and has been considered a potential target for antifungal therapies.[23] The precise biological significance of HSP up-regulation deserves further investigation.

In the acetylome analysis, 5,580 acetylated sites were identified on 2,422 proteins. Among these acetylated proteins, 503 proteins were not identified in the whole-cell proteome, possibly due to their relatively low expression levels, leading them to escape detection in our shotgun proteome analysis. Acetylated proteins with low abundance may be identified using an acetylated peptide enrichment strategy, which could expand the proteins identified in the whole-cell proteome.

In total, 386 acetylated sites on 285 proteins were identified in the conidial stage, and 5,414 acetylated sites on 2,335 proteins were identified in the mycelial stage, suggesting that 92% of the identified acetylated proteins and 96% of acetylated sites were growth-stage specific (Figure S7A). Although there were significant differences in acetylation modifications between the conidial and mycelial stages, the GO classification showed a similar distribution of acetylated proteins in the majority of categories between the two stages; thus, acetylated proteins are highly involved in

metabolism, translation and macromolecule biosynthetic processes. These results suggest conserved roles for acetylation modifications in these two stages of *T. rubrum*. However, some differences also exist, including the differentially enriched KEGG pathways for acetylated proteins and the different acetylation modification sites on histones, suggesting that acetylation is differentially involved in some metabolic pathways and participates in epigenetic regulation in distinct ways between the two stages. Moreover, the different amino acid sequence features in the vicinity of the Kac sites observed between the two stages suggest that the enzymes that regulate acetylation may function in a growth-stage-specific manner.

Compared with succinylation in *T. rubrum*, 231 proteins and 257 sites were observed to be simultaneously modified by the two kinds of PTMs. These two PTMs were shown to be commonly involved in some fundamental essential pathways based on KEGG enrichment, although there were also specific roles for each PTM. Based on secondary structure analysis, the acetylation- and succinylation-modified sites showed differences in surface accessibility; succinylated lysines tended to be exposed on the protein surface, while acetylated lysines were less likely to be exposed on the protein surface compared with all lysines. Furthermore, based on subcellular localization analysis, the cytosol and nucleus were the largest categories of acetylated proteins in conidia and mycelia, respectively. This distribution of acetylated proteins was different from that of succinylated proteins, which were most frequently located in the mitochondria because the mitochondria are the major provenance for succinyl-CoA. Succinylation outside of mitochondria is catalyzed by succinyl-CoA,

which traverses the mitochondrial membrane or forms as a side-product of ketoglutarate-dependent enzymes.[45] For acetylation, it has been suggested that the nucleus/cytosol and mitochondria exhibit distinct acetyl-CoA pools in eukaryotic systems and that acetyl-CoA is catalyzed by distinct enzymes in the nucleus/cytosol and mitochondria; also, acetyl-CoA is not freely exchanged between the mitochondria and other cellular compartments.[46]

The succinylation results showed similar abundance between the conidial and mycelial stages, but acetylation was much more abundant in mycelia than in conidia. To investigate whether the difference in acetylation abundance is caused by a difference in protein abundance in the two stages, the acetylome and the proteome were compared. There was a slight preference for the acetylation modification on relatively more-abundant proteins in the two stages, but no significant correlation between acetylation and protein abundance was found. These results suggest that acetylation modifications are growth-stage specific and show a preference for modifying proteins that is not dependent on protein abundance.

Consistent with the finding that acetylation was more abundant in the mycelial stage, acetyltransferases were greatly enriched among proteins specific to the mycelial stage in the whole-cell proteome analysis. Lysine acetylation is dynamically regulated by the balance of lysine acetyltransferases (KATs) and lysine deacetylases (KDACs). KATs catalyze the transfer of an acetyl group to the lysine ε-amino side-chain in proteins. These enzymes can be grouped into the following three major families: (1) MYST (Moz, Ybf2, Sas2 and Tip60), (2) GNAT (Gcn5-related N-acetyltransferase)

and (3) p300/CREB-binding proteins (p300/CBP).[47] With the opposing activity of acetyltransferases, KDACs catalyze the removal of acetyl groups from substrate proteins. KDACs can be classified into the following two families: (1) Zn^{2+}-dependent histone deacetylases (HDAC) and (2) NAD^{+}-dependent sirtuin deacetylases (SIRT1–7).[47] In our whole-cell proteome analysis, 31 possible lysine acetyltransferases and 8 possible deacetylases were identified. Our results showed that most acetyltransferases were specific to or more abundant in the mycelial stage. Among the deacetylases identified in our study, three enzymes were more abundant in mycelia, and five enzymes showed no significant differences between the two stages. The differences in acetylation between the two stages are a consequence of control by these two opposing enzymes.

Our results showed that inhibition of KATs or KDACs had significant antifungal effect and induced cell apoptosis. Several inhibitors of KATs and KDACs are already in use or considered as potential reagent for antitumor therapy. Several of these inhibitors have limited or only little effect on normal cells.[42] In addition, some KATs and KDACs in filamentous fungi are relative lowly homologous with their counterparts in human cell. For instance, the deactylase RpdA has several amino residues in the C-terminal which are specific to filamentous fungi. This filamentous fungi specific C-terminal region are essential for the enzymatic activity of RpdA as well as fungal vitality, making this C-terminal region a promising target for designing KDACs inhibitor.[42] In addition, HOS3 are fungal specific deacetylase that had been reported in Candida and filamentous fungi.[48] Therefore, designation of fungal specific

KATs and KDACs inhibitors or testing more inhibitors which are less harmful to human cell are desirable approach to antifungal therapy.

5. Conclusions

Our results provide new insights about *T. rubrum* and reveal many essential features of and differences between its two major growth stages, based on whole-cell proteome and acetylome analyses. Especially, disruption of balanced acetylation level significantly inhibited fungal growth and induced cell apoptosis. These data will improve our understanding of the biological properties of *T. rubrum* and other closely related dermatophytes, which will provide a solid foundation for developing advanced therapies targeting these important pathogenic fungi.

ASSOCIATED CONTENT

The mass spectrometry data of our study has been deposited in the publicly accessible database PeptideAtlas. The proteome data is available with dataset identifier PASS01111 (dataset password: xu000000), and the acetylome dataset is available with the identifier PASS01109 (dataset password: xu000000).

Supporting Information.

Figure S1. The GO classification of the proteins identified in the whole-cell proteome in conidia and mycelia respectively (PDF)

Figure S2. The ratio of protein abundance in the mycelial vs. conidial stage for all the quantified proteins (PDF)

Figure S3. The repeatability of quantification of the whole-cell proteome analysis (PDF)

Figure S4. KEGG enrichment of proteins identified in the whole-cell proteome analysis (PDF)

Figure S5. Validation of label free quantification by qRT-PCR (PDF)

Figure S6. Venn diagram of the identified acetylated proteins and sites in each replicate (PDF)

Figure S7. The acetylated proteins and sites identified in *T. rubrum* (PDF)

Figure S8. GO and KEGG enrichment analysis of the acetylated proteins (PDF)

Table S1. PRM assay to validate the results of whole-cell proteome (XLSX)

Table S2. Primers used in the quantitative real-time PCR assays (XLSX)

Table S3. Proteins identified in the whole-cell proteome (XLSX)

Table S4. GO enrichment of proteins identified in the whole-cell proteome (XLSX)

Table S5. KEGG enrichment of proteins identified in the whole-cell proteome (XLSX)

Table S6. Acetylated proteins and sites identified in conidia and mycelia (XLSX)

Table S7. GO and subcellular location classification of the acetylated proteins (XLSX)

Table S8. GO and KEGG enrichment of acetylated proteins (XLSX)

Table S9. The identified acetylated proteins related to fungal pathogenicity (XLSX)

Table S10. Amino acid sequence motif surrounding the Kac conserved in conidia and mycelia (XLSX)

Table S11. Conservation of acetylated proteins in *T. rubrum* and other species (XLSX)

Table S12. Cross-talk between acetylation and succinylation in *T. rubrum* (XLSX)

AUTHOR INFORMATION

Corresponding Author

*(Q.J.) E-mail: zdsys@vip.sina.com, Telephone: +86-10-67877732, Fax: +86-10-67877736.

Author Contributions

The manuscript was written through contributions of all authors. All authors have given approval to the final version of the manuscript. ‡These authors contributed equally.

Notes

The authors declare no competing financial interest.

ACKNOWLEDGMENT

This work was supported by the CAMS Innovation Fund for Medical Sciences

(CIFMS) (Grant No. 2016-I2M-3-021).

REFERENCES

(1) Zamani, S.; Sadeghi, G.; Yazdinia, F.; Moosa, H.; Pazooki, A.; Ghafarinia, Z.; Abbasi, M.; Shams-Ghahfarokhi, M.; Razzaghi-Abyaneh, M. Epidemiological trends of dermatophytosis in Tehran, Iran: A five-year retrospective study. *J. Mycol. Med.* **2016**, *26* (4), 351-358.

(2) Yoshikawa, F. S.; Yabe, R.; Iwakura, Y.; de Almeida, S. R.; Saijo, S. Dectin-1 and Dectin-2 promote control of the fungal pathogen Trichophyton rubrum independently of IL-17 and adaptive immunity in experimental deep dermatophytosis. *Innate Immun.* **2016**, *22* (5), 316-324.

(3) Mordorski, B.; Costa-Orlandi, C. B.; Baltazar, L. M.; Carreno, L. J.; Landriscina, A.; Rosen, J.; Navati, M.; Mendes-Giannini, M. J. S.; Friedman, J. M.; Nosanchuk, J. D.; Friedman, A. J. Topical nitric oxide releasing nanoparticles are effective in a murine model of dermal Trichophyton rubrum dermatophytosis. *Nanomedicine* **2017**, *13* (7), 2267-2270.

(4) Afshari, M. A.; Shams-Ghahfarokhi, M.; Razzaghi-Abyaneh, M. Antifungal susceptibility and virulence factors of clinically isolated dermatophytes in Tehran, Iran. *Iran J. Microbiol.* **2016**, *8* (1), 36-46.

(5) Barros, B. H.; da Silva, S. H.; dos ReisMarques Edos, R.; Rosa, J. C.; Yatsuda, A. P.; Roberts, D. W.; Braga, G. U. A proteomic approach to identifying proteins differentially expressed in conidia and mycelium of the entomopathogenic fungus

Metarhizium acridum. *Fungal Biol.* **2010**, *114* (7), 572-579.

(6) Liu, T.; Zhang, Q.; Wang, L.; Yu, L.; Leng, W.; Yang, J.; Chen, L.; Peng, J.; Ma, L.; Dong, J.; Xu, X.; Xue, Y.; Zhu, Y.; Zhang, W.; Yang, L.; Li, W.; Sun, L.; Wan, Z.; Ding, G.; Yu, F.; Tu, K.; Qian, Z.; Li, R.; Shen, Y.; Li, Y.; Jin, Q. The use of global transcriptional analysis to reveal the biological and cellular events involved in distinct development phases of Trichophyton rubrum conidial germination. *BMC Genomics* **2007**, *8*, 100.

(7) Bhadauria, V.; Zhao, W. S.; Wang, L. X.; Zhang, Y.; Liu, J. H.; Yang, J.; Kong, L. A.; Peng, Y. L. Advances in fungal proteomics. *Microbiol. Res.* **2007**, *162* (3), 193-200.

(8) Zhang, K.; Zheng, S.; Yang, J. S.; Chen, Y.; Cheng, Z. Comprehensive profiling of protein lysine acetylation in Escherichia coli. *J. Proteome Res.* **2013**, *12* (2), 844-851.

(9) He, M.; Han, Z.; Liu, L.; Zheng, Y. G. Chemical Biology for Investigating Epigenetic Functions of Lysine Acetyltransferases (KATs). *Angew. Chem. Int. Ed. Engl.* **2017**.

(10) Lv, B.; Yang, Q.; Li, D.; Liang, W.; Song, L. Proteome-wide analysis of lysine acetylation in the plant pathogen Botrytis cinerea. *Sci. Rep.* **2016**, *6*, 29313.

(11) Leng, W.; Liu, T.; Li, R.; Yang, J.; Wei, C.; Zhang, W.; Jin, Q. Proteomic profile of dormant Trichophyton rubrum conidia. *BMC Genomics* **2008**, *9*, 303.

(12) Xu, X.; Liu, T.; Yang, J.; Chen, L.; Liu, B.; Wei, C.; Wang, L.; Jin, Q. The first succinylome profile of Trichophyton rubrum reveals lysine succinylation on proteins

involved in various key cellular processes. *BMC Genomics* **2017**, *18* (1), 577.

(13) Tyanova, S.; Temu, T.; Cox, J. The MaxQuant computational platform for mass spectrometry-based shotgun proteomics. *Nat. Protoc.* **2016**, *11* (12), 2301-2319.

(14) NCCLS. Reference Method for Broth Dilution Antifungal Susceptibility Testing of Conidium-forming Filamentous Fungi. Proposed Standard M38-A. Wayne, PA. **2002**.

(15) You, B. J.; Lee, M. H.; Tien, N.; Lee, M. S.; Hsieh, H. C.; Tseng, L. H.; Chung, Y. L.; Lee, H. Z. A novel approach to enhancing ganoderic acid production by Ganoderma lucidum using apoptosis induction. *PLoS One* **2013**, *8* (1), e53616.

(16) Bitencourt, T. A.; Komoto, T. T.; Massaroto, B. G.; Miranda, C. E.; Beleboni, R. O.; Marins, M.; Fachin, A. L. Trans-chalcone and quercetin down-regulate fatty acid synthase gene expression and reduce ergosterol content in the human pathogenic dermatophyte Trichophyton rubrum. *BMC Complement Altern. Med.* **2013**, *13*, 229.

(17) Rezende, T. C.; Borges, C. L.; Magalhaes, A. D.; de Sousa, M. V.; Ricart, C. A.; Bailao, A. M.; Soares, C. M. A quantitative view of the morphological phases of Paracoccidioides brasiliensis using proteomics. *J. Proteomics* **2011**, *75* (2), 572-587.

(18) Monod, M. Secreted proteases from dermatophytes. *Mycopathologia* **2008**, *166* (5-6), 285-294.

(19) Scharf, D. H.; Heinekamp, T.; Brakhage, A. A. Human and plant fungal pathogens: the role of secondary metabolites. *PLoS Pathog.* **2014**, *10* (1), e1003859.

(20) Sbaraini, N.; Andreis, F. C.; Thompson, C. E.; Guedes, R. L. M.; Junges, A.; Campos, T.; Staats, C. C.; Vainstein, M. H.; Ribeiro de Vasconcelos, A. T.; Schrank, A.

Genome-Wide Analysis of Secondary Metabolite Gene Clusters in Ophiostoma ulmi and Ophiostoma novo-ulmi Reveals a Fujikurin-Like Gene Cluster with a Putative Role in Infection. *Front. Microbiol.* **2017**, *8*, 1063.

(21) Riquelme, M.; Martinez-Nunez, L. Hyphal ontogeny in Neurospora crassa: a model organism for all seasons. *F1000Res.* **2016**, *5*, 2801.

(22) Haag, C.; Steuten, B.; Feldbrugge, M. Membrane-Coupled mRNA Trafficking in Fungi. *Annu. Rev. Microbiol.* **2015**, *69*, 265-281.

(23) Jacob, T. R.; Peres, N. T.; Martins, M. P.; Lang, E. A.; Sanches, P. R.; Rossi, A.; Martinez-Rossi, N. M. Heat Shock Protein 90 (Hsp90) as a Molecular Target for the Development of Novel Drugs Against the Dermatophyte Trichophyton rubrum. *Front. Microbiol.* **2015**, *6*, 1241.

(24) Zhou, X.; Qian, G.; Yi, X.; Li, X.; Liu, W. Systematic Analysis of the Lysine Acetylome in Candida albicans. *J. Proteome Res.* **2016**, *15* (8), 2525-2536.

(25) Henriksen, P.; Wagner, S. A.; Weinert, B. T.; Sharma, S.; Bacinskaja, G.; Rehman, M.; Juffer, A. H.; Walther, T. C.; Lisby, M.; Choudhary, C. Proteome-wide analysis of lysine acetylation suggests its broad regulatory scope in Saccharomyces cerevisiae. *Mol. Cell. Proteomics* **2012**, *11* (11), 1510-1522.

(26) Li, D.; Lv, B.; Tan, L.; Yang, Q.; Liang, W. Acetylome analysis reveals the involvement of lysine acetylation in diverse biological processes in Phytophthora sojae. *Sci. Rep.* **2016**, *6*, 29897.

(27) Hong, Y.; Cao, X.; Han, Q.; Yuan, C.; Zhang, M.; Han, Y.; Zhu, C.; Lin, T.; Lu, K.; Li, H.; Fu, Z.; Lin, J. Proteome-wide analysis of lysine acetylation in adult

Schistosoma japonicum worm. *J. Proteomics* **2016**, *148*, 202-212.

(28) Guo, J.; Wang, C.; Han, Y.; Liu, Z.; Wu, T.; Liu, Y.; Liu, Y.; Tan, Y.; Cai, X.; Cao, Y.; Wang, B.; Zhang, B.; Liu, C.; Tan, S.; Zhang, T. Identification of Lysine Acetylation in Mycobacterium abscessus Using LC-MS/MS after Immunoprecipitation. *J. Proteome Res.* **2016**, *15* (8), 2567-2578.

(29) Sriranganadane, D.; Waridel, P.; Salamin, K.; Feuermann, M.; Mignon, B.; Staib, P.; Neuhaus, J. M.; Quadroni, M.; Monod, M. Identification of novel secreted proteases during extracellular proteolysis by dermatophytes at acidic pH. *Proteomics* **2011**, *11* (22), 4422-4433.

(30) Cornet, M.; Gaillardin, C. pH signaling in human fungal pathogens: a new target for antifungal strategies. *Eukaryot. Cell* **2014**, *13* (3), 342-352.

(31) Godinho, R. M.; Crestani, J.; Kmetzsch, L.; Araujo Gde, S.; Frases, S.; Staats, C. C.; Schrank, A.; Vainstein, M. H.; Rodrigues, M. L. The vacuolar-sorting protein Snf7 is required for export of virulence determinants in members of the Cryptococcus neoformans complex. *Sci. Rep.* **2014**, *4*, 6198.

(32) Costa, C.; Dias, P. J.; Sa-Correia, I.; Teixeira, M. C. MFS multidrug transporters in pathogenic fungi: do they have real clinical impact? *Front. Physiol.* **2014**, *5*, 197.

(33) Kurdistani, S. K.; Grunstein, M. Histone acetylation and deacetylation in yeast. *Nat. Rev. Mol. Cell Biol.* **2003**, *4* (4), 276-284.

(34) Leach, M. D.; Brown, A. J. Posttranslational modifications of proteins in the pathobiology of medically relevant fungi. *Eukaryot. Cell* **2012**, *11* (2), 98-108.

(35) Liu, Z.; Wang, Y.; Gao, T.; Pan, Z.; Cheng, H.; Yang, Q.; Cheng, Z.; Guo, A.;

Ren, J.; Xue, Y. CPLM: a database of protein lysine modifications. *Nucleic Acids Res.* **2014**, *42* (Database issue), D531-536.

(36) Liu, Z.; Cao, J.; Gao, X.; Zhou, Y.; Wen, L.; Yang, X.; Yao, X.; Ren, J.; Xue, Y. CPLA 1.0: an integrated database of protein lysine acetylation. *Nucleic Acids Res.* **2011**, *39* (Database issue), D1029-1034.

(37) Xu, H.; Zhou, J.; Lin, S.; Deng, W.; Zhang, Y.; Xue, Y. PLMD: An updated data resource of protein lysine modifications. *J. Genet. Genomics* **2017**, *44* (5), 243-250.

(38) Liu, F.; Yang, M.; Wang, X.; Yang, S.; Gu, J.; Zhou, J.; Zhang, X. E.; Deng, J.; Ge, F. Acetylome analysis reveals diverse functions of lysine acetylation in Mycobacterium tuberculosis. *Mol. Cell. Proteomics* **2014**, *13* (12), 3352-3366.

(39) Weinert, B. T.; Scholz, C.; Wagner, S. A.; Iesmantavicius, V.; Su, D.; Daniel, J. A.; Choudhary, C. Lysine succinylation is a frequently occurring modification in prokaryotes and eukaryotes and extensively overlaps with acetylation. *Cell Rep.* **2013**, *4* (4), 842-851.

(40) Gu, M. L.; Wang, Y. M.; Zhou, X. X.; Yao, H. P.; Zheng, S.; Xiang, Z.; Ji, F. An inhibitor of the acetyltransferases CBP/p300 exerts antineoplastic effects on gastrointestinal stromal tumor cells. *Oncol. Rep.* **2016**, *36* (5), 2763-2770.

(41) Mottamal, M.; Zheng, S.; Huang, T. L.; Wang, G. Histone deacetylase inhibitors in clinical studies as templates for new anticancer agents. *Molecules* **2015**, *20* (3), 3898-3941.

(42) Bauer, I.; Varadarajan, D.; Pidroni, A.; Gross, S.; Vergeiner, S.; Faber, B.; Hermann, M.; Tribus, M.; Brosch, G.; Graessle, S. A Class 1 Histone Deacetylase

with Potential as an Antifungal Target. *MBio* **2016**, *7* (6).

(43) Ishaque, A.; Al-Rubeai, M. Use of intracellular pH and annexin-V flow cytometric assays to monitor apoptosis and its suppression by bcl-2 over-expression in hybridoma cell culture. *J. Immunol. Methods* **1998**, *221* (1-2), 43-57.

(44) Martinez-Rossi, N. M.; Jacob, T. R.; Sanches, P. R.; Peres, N. T.; Lang, E. A.; Martins, M. P.; Rossi, A. Heat Shock Proteins in Dermatophytes: Current Advances and Perspectives. *Curr. Genomics* **2016**, *17* (2), 99-111.

(45) Hausinger, R. P. FeII/alpha-ketoglutarate-dependent hydroxylases and related enzymes. *Crit. Rev. Biochem. Mol. Biol.* **2004**, *39* (1), 21-68.

(46) Albaugh, B. N.; Arnold, K. M.; Denu, J. M. KAT(ching) metabolism by the tail: insight into the links between lysine acetyltransferases and metabolism. *Chembiochem.* **2011**, *12* (2), 290-298.

(47) Sabari, B. R.; Zhang, D.; Allis, C. D.; Zhao, Y. Metabolic regulation of gene expression through histone acylations. *Nat. Rev.. Mol. Cell Biol.* **2017**, *18* (2), 90-101.

(48) Brosch, G.; Loidl, P.; Graessle, S. Histone modifications and chromatin dynamics: a focus on filamentous fungi. *FEMS Microbiol. Rev.* **2008**, *32* (3), 409-439.

Figure legends

Figure 1. GO enrichment of proteins in the whole-cell proteome analysis. Enrichment analysis was performed based on the biological process (red bar), molecular function (yellow bar) and cellular component (green bar) categories. (A) GO enrichment of conidium-specific proteins. (B) GO enrichment of the mycelium-specific proteins. (C) GO enrichment of differentially expressed proteins.

Figure 2. Classification of acetylated proteins based on GO (biological process, molecular function and cellular component) and subcellular location. (A) Classification of acetylated proteins in the conidial stage. (B) Classification of acetylated proteins in the mycelial stage.

Figure 3. Histone acetylation modifications. (A) Identified acetylation sites (shown in bold red font.) on histones and the conservation in other species. The letter "B" in brackets indicates that the site is modified in both the conidial and mycelial stages, and the letter "M" in brackets indicates that the site is modified only in the mycelial stage. (B) Western blot validation of two acetylated sites.

Figure 4. Heat maps showing the frequency of the amino acids present surrounding acetylated sites. (A) Conidial stage. (B) Mycelial stage. The colors represent the enrichment (red) or depletion (green) of amino acids at the specific positions.

Figure 5. Distribution of acetylated lysines (indicated with a green bar) and all lysines (indicated in blue) in protein secondary structures (α-helices, β-strands, and coils) and their surface accessibility.

Figure 6. Venn diagrams showing the overlapping acetylated proteins in *T. rubrum*

and other organisms.

Figure 7. Heat map showing the relationship between acetylation and succinylation modifications based on KEGG enrichment. The colors represent the enrichment (red) or depletion (green) of the pathway for each type.

Figure 8. Fungal viability and apoptosis assay with the treatment of KATs and KDACs inhibitors. (A) Fungal viability assay. *T. rubrum* were treated with different concentration of each inhibitor in 0.1% DMSO, compared to control treated with 0.1% DMSO. Fungal viability were measured by XTT assay. Each bar represents the mean ± SD from three replicates ($P < 0.01$). (B) Histogram of apoptotic rate evaluated by TUNEL assay. Mycelia were treated with each inhibitor at MIC for 2 h, compared to the control treated with 0.1% DMSO. Each sample were double stained with DAPI and TUNEL. The apoptotic rate was determined by scoring the percentage of cells with green fluorescence (TUNEL positive) in total DAPI-stained ones. Three replicates were performed ($P< 0.01$). (C) TUNEL assay visualized with fluorescence microscopy. (D) Apoptotic rate evaluated by Annxin V-FITC/PI staining. Protoplasts were treated with each inhibitor at 0.5 MIC for 2 h, compared to control treated with 0.1% DMSO. Protoplasts were double stained with Annxin V-FITC/PI and then subjected to flow cytometry analysis. Four quadrants in each histogram indicated different type of cell population: Q3 (Annexin V-FITC-/PI-), viable cell; Q4 (Annexin V-FITC+/PI-), early apoptotic cell; Q2 (Annexin V-FITC+/PI+), late apoptotic cell; and Q1 (Annexin V-FITC-/PI+), necrotic cell.

Table 1. The comparison of the quantification results between the label free and PRM methods.

Protein Accession	Protein names	Fold change (mycelia/conidia) in PRM	Fold change (mycelia/conidia) in label free
TERG_00189T0	40S ribosomal protein S0	2.01±0.16	3.43±0.67
TERG_00633T0	40S ribosomal protein S9	1.91±0.37	4.69±1.61
TERG_00720T0	Ribosomal protein L19	10.59±1.05	9.78±2.07
TERG_01574T0	40S ribosomal protein S13	8.17±0.34	15.20±6.15
TERG_01883T0	Hsp70 chaperone	3.05±0.35	7.29±1.56
TERG_02032T0	ATP synthase subunit alpha	3.35±0.15	4.23±0.08
TERG_02486T0	Eukaryotic translation initiation factor subunit eIF2A	4.09±0.51	5.85±1.29
TERG_06963T0	Molecular chaperone Mod-E/Hsp90	4.87±0.37	13.47±4.50
TERG_01281T0	Malate synthase	0.07±0.00	0.08±0.00
TERG_04338T0	Alkaline protease 2	0.41±0.05	0.46±0.08
TERG_05304T0	Cyanate hydratase	0.04±0.00	0.05±0.02
TERG_06625T0	Tripeptidyl peptidase SED3	0.05±0.00	0.01±0.00
TERG_00216T0	Class V chitinase	0.00	0.00
TERG_06780T0	GPI anchored cell wall protein	0.00	0.00

The fold change is illustrated as the mean ± SD ($P < 0.05$).

Table 2. The antifungal activity of inhibitors of KATs and HDACs by micro-broth dilution assay.

Inhibitors	MIC[a]	MFC[b]
KATs inhibitors		
MG149	10μM	30μM
Remodelin	10μM	ND[c]
HDACs inhibitors		
TSA	5μM	20μM
LBH589	10μM	ND

[a]MIC, minimal inhibitory concentration; [b]MFC, minimal fungicidal concentration; [c]ND, not determined with the tested concentration.

Figure 1

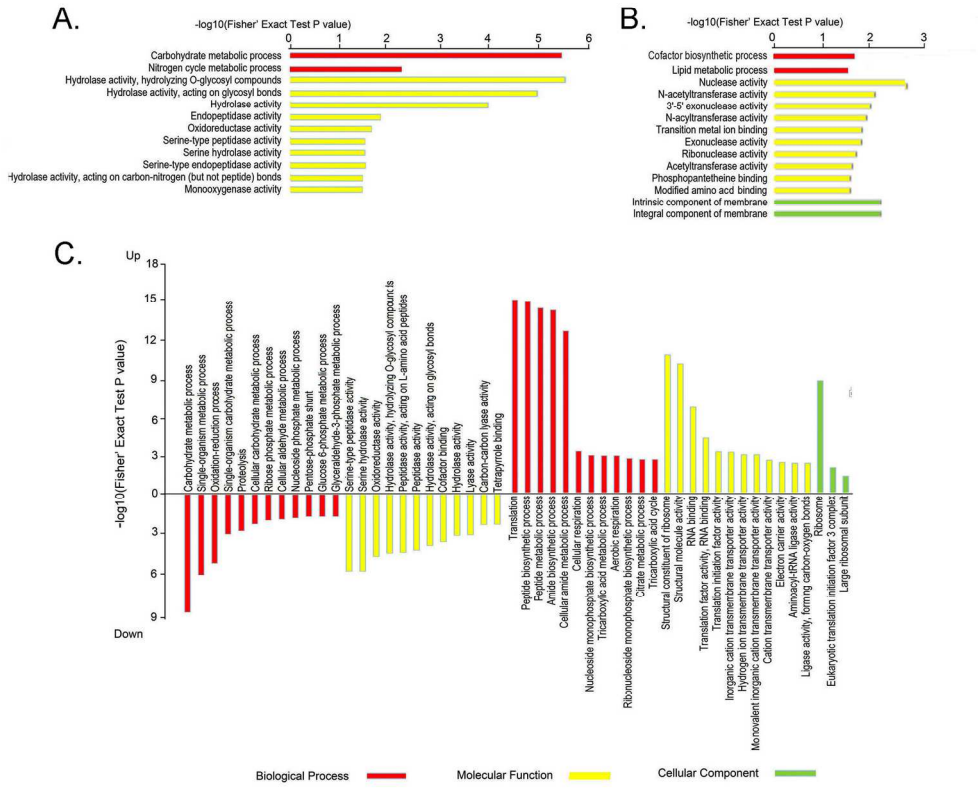

Figure 1. GO enrichment of proteins in the whole-cell proteome analysis. Enrichment analysis was performed based on the biological process (red bar), molecular function (yellow bar) and cellular component (green bar) categories. (A) GO enrichment of conidium-specific proteins. (B) GO enrichment of the mycelium-specific proteins. (C) GO enrichment of differentially expressed proteins.

177x156mm (300 x 300 DPI)

Figure 2

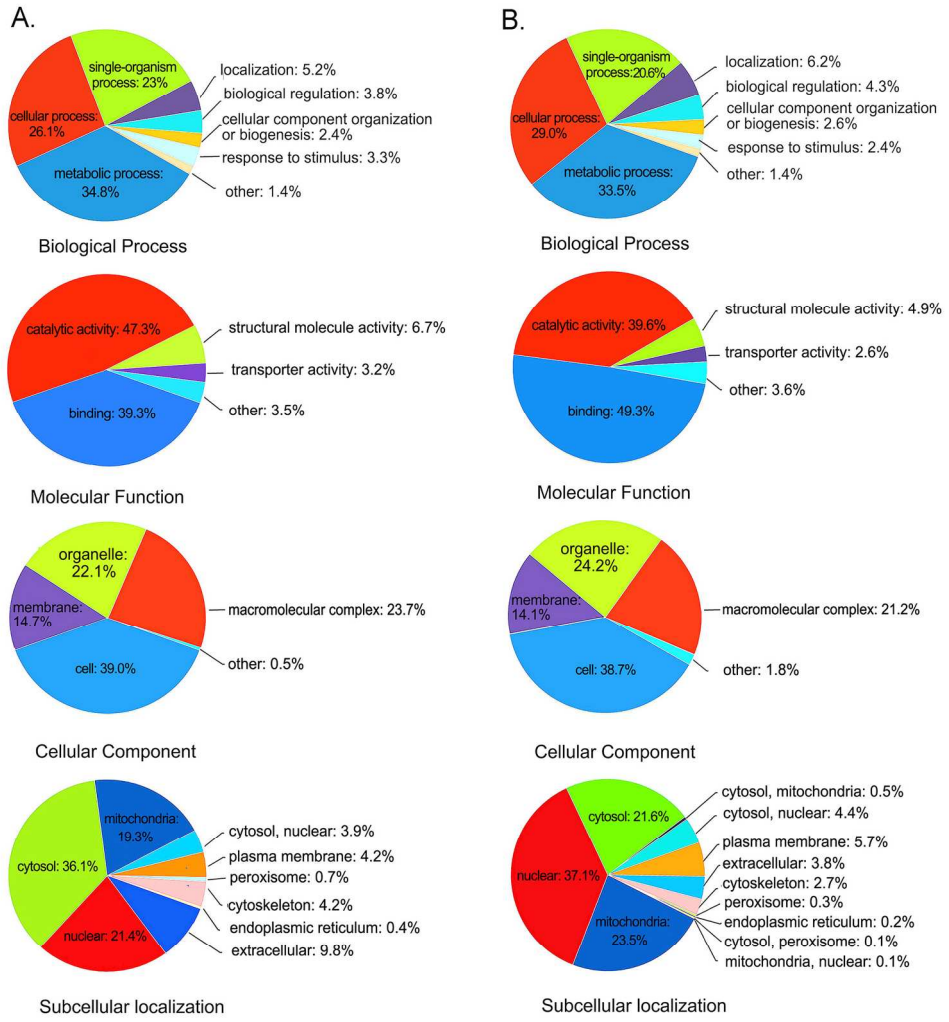

Figure 2. Classification of acetylated proteins based on GO (biological process, molecular function and cellular component) and subcellular location. (A) Classification of acetylated proteins in the conidial stage. (B) Classification of acetylated proteins in the mycelial stage.

175x204mm (300 x 300 DPI)

Figure 3

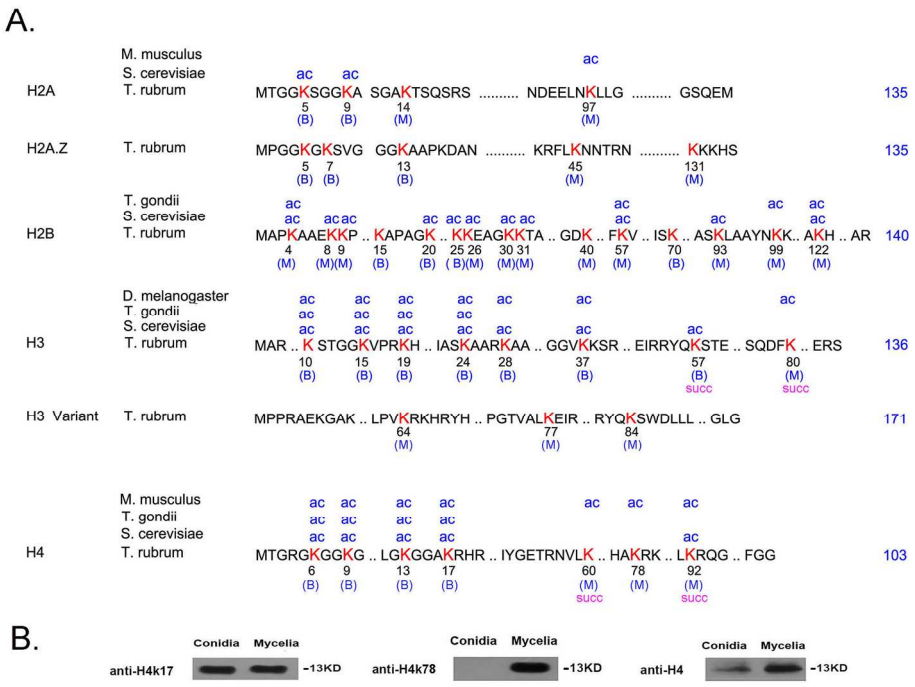

Figure 3. Histone acetylation modifications. (A) Identified acetylation sites (shown in bold red font.) on histones and the conservation in other species. The letter "B" in brackets indicates that the site is modified in both the conidial and mycelial stages, and the letter "M" in brackets indicates that the site is modified only in the mycelial stage. (B) Western blot validation of two acetylated sites.

177x143mm (300 x 300 DPI)

Figure 4

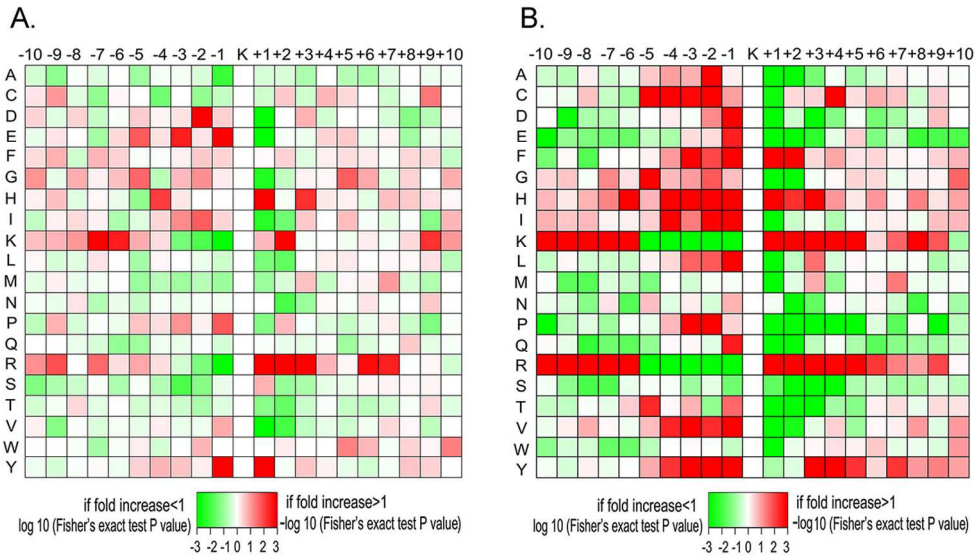

Figure 4. Heat maps showing the frequency of the amino acids present surrounding acetylated sites. (A) Conidial stage. (B) Mycelial stage. The colors represent the enrichment (red) or depletion (green) of amino acids at the specific positions.

123x77mm (300 x 300 DPI)

Figure 5

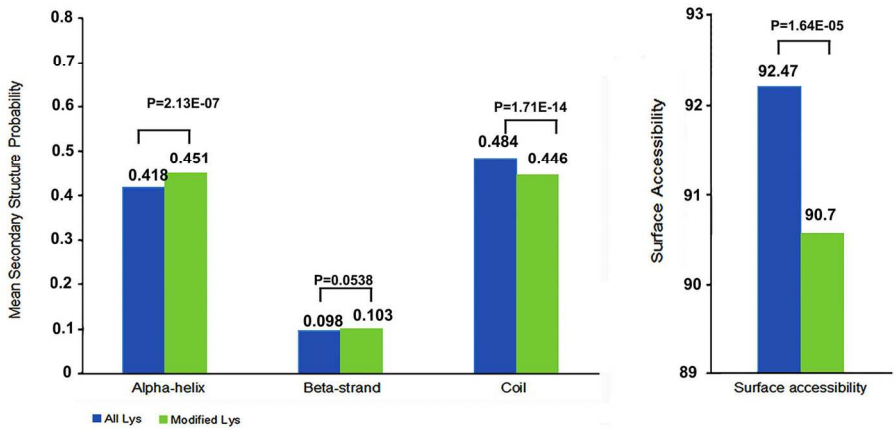

Figure 5. Distribution of acetylated lysines (indicated with a green bar) and all lysines (indicated in blue) in protein secondary structures (α-helices, β-strands, and coils) and their surface accessibility.

153x89mm (300 x 300 DPI)

Figure 6

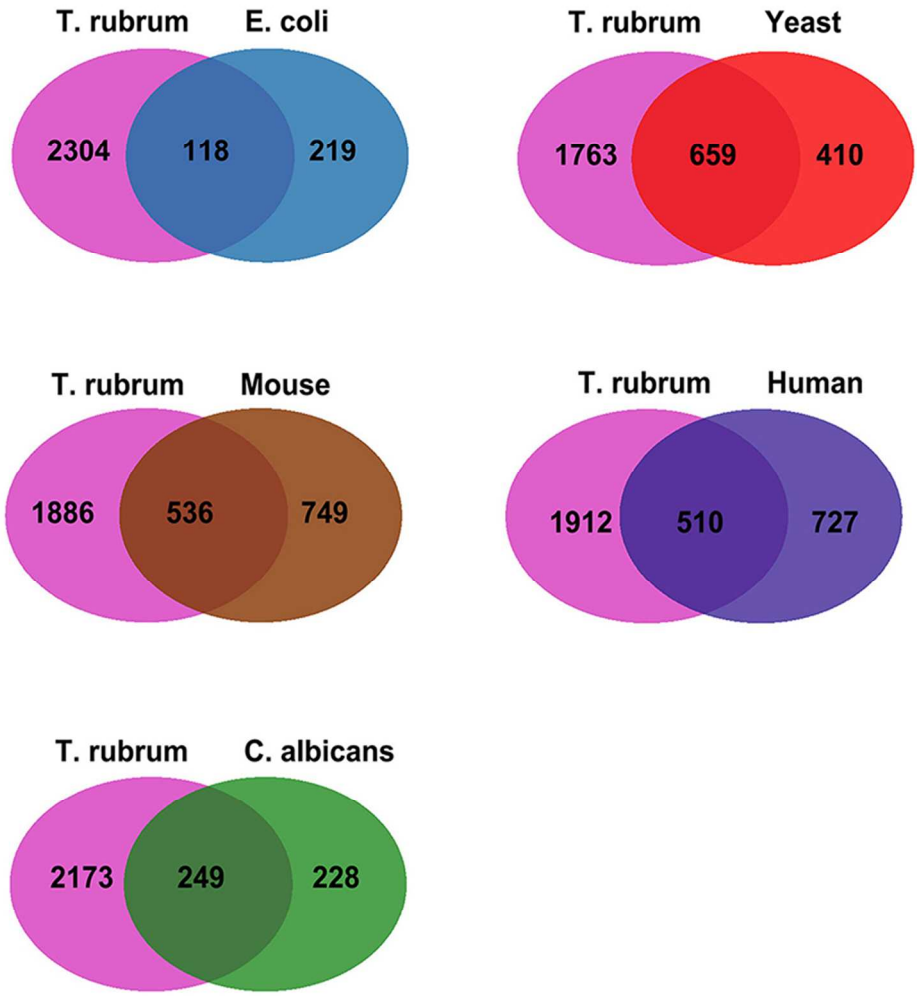

Figure 6. Venn diagrams showing the overlapping acetylated proteins in T. rubrum and other organisms.

73x90mm (300 x 300 DPI)

Figure 7

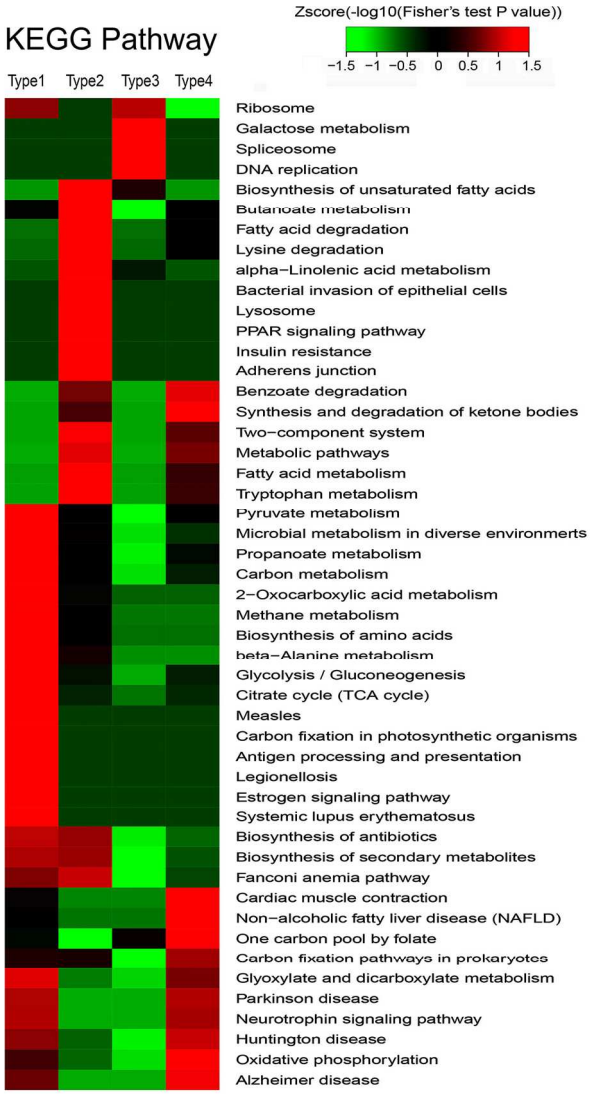

Figure 7. Heat map showing the relationship between acetylation and succinylation modifications based on KEGG enrichment. The colors represent the enrichment (red) or depletion (green) of the pathway for each type.

109x199mm (300 x 300 DPI)

Figure 8

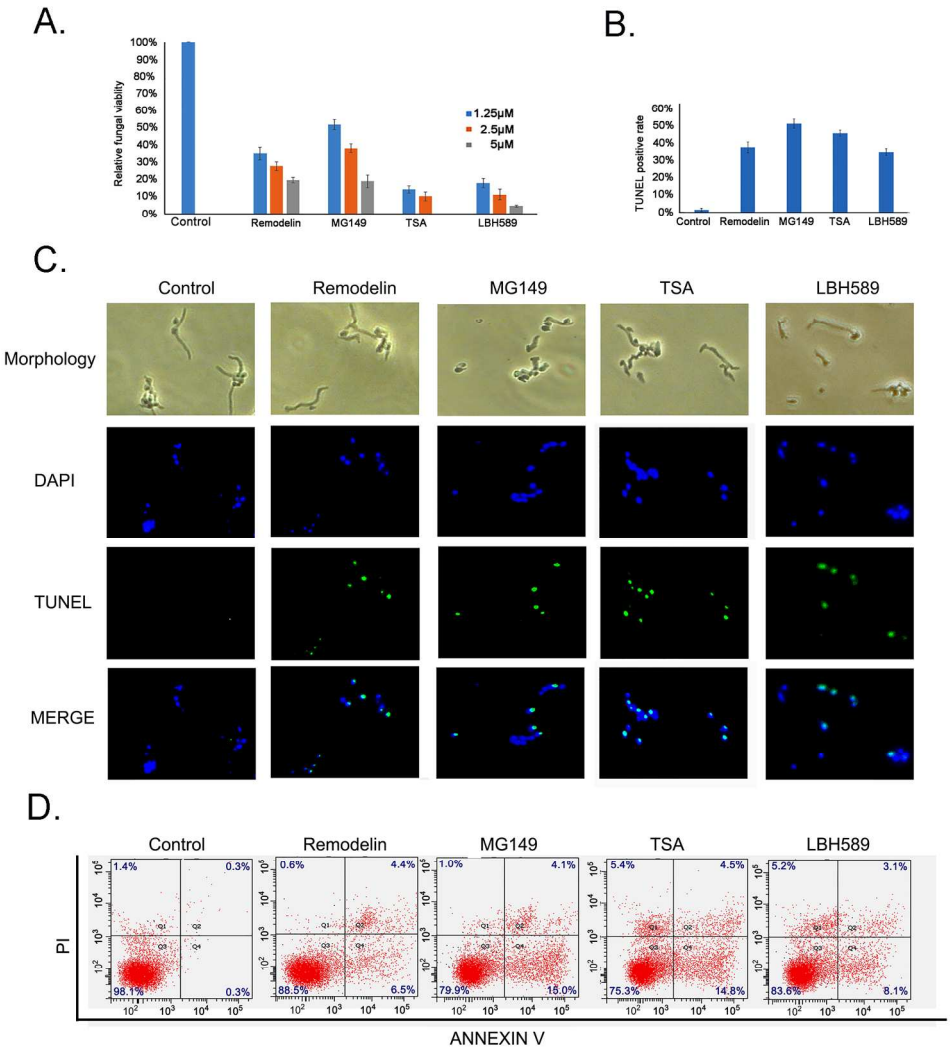

Figure 8. Fungal viability and apoptosis assay with the treatment of KATs and KDACs inhibitors. (A) Fungal viability assay. T. rubrum were treated with different concentration of each inhibitor in 0.1% DMSO, compared to control treated with 0.1% DMSO. Fungal viability were measured by XTT assay. Each bar represents the mean ± SD from three replicates ($P < 0.01$). (B) Histogram of apoptotic rate evaluated by TUNEL assay. Mycelia were treated with each inhibitor at MIC for 2 h, compared to the control treated with 0.1% DMSO. Each sample were double stained with DAPI and TUNEL. The apoptotic rate was determined by scoring the percentage of cells with green fluorescence (TUNEL positive) in total DAPI-stained ones. Three replicates were performed ($P< 0.01$). (C) TUNEL assay visualized with fluorescence microscopy. (D) Apoptotic rate evaluated by Annxin V-FITC/PI staining. Protoplasts were treated with each inhibitor at 0.5 MIC for 2 h, compared to control treated with 0.1% DMSO. Protoplasts were double stained with Annxin V-FITC/PI and then subjected to flow cytometry analysis. Four quadrants in each histogram indicated different type of cell population: Q3 (Annexin V-FITC-/PI-), viable cell; Q4 (Annexin V-FITC+/PI-), early apoptotic cell; Q2 (Annexin V-FITC+/PI+), late apoptotic cell; and Q1 (Annexin V-FITC-/PI+), necrotic cell.

177x209mm (300 x 300 DPI)

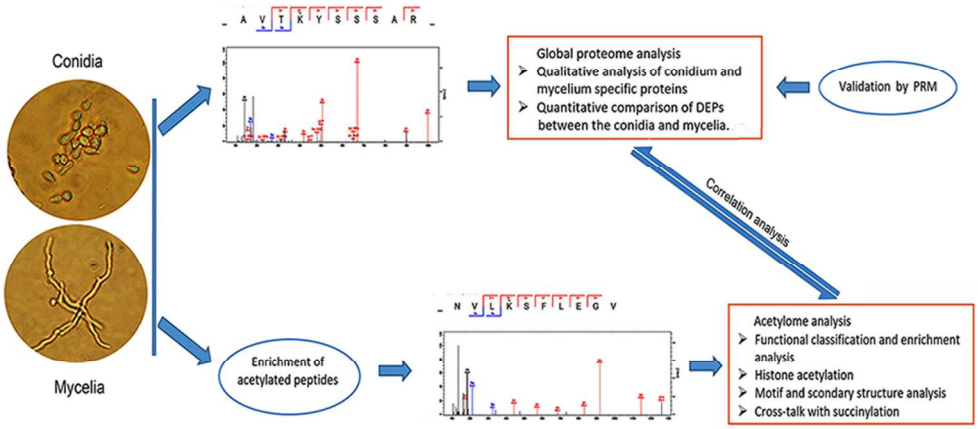

Abstract Graphic_for TOC only

82x40mm (300 x 300 DPI)